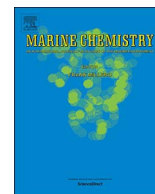




Contents lists available at ScienceDirect

Marine Chemistry

journal homepage: www.elsevier.com/locate/marchem

On the influence of marine biogeochemical processes over CO₂ exchange between the atmosphere and ocean

Matthew P. Humphreys^{a,b,*}, Chris J. Daniels^c, Dieter A. Wolf-Gladrow^d, Toby Tyrrell^a,
Eric P. Achterberg^{a,e}

^a Ocean and Earth Science, National Oceanography Centre Southampton, University of Southampton, Waterfront Campus, European Way, Southampton SO14 3ZH, UK

^b School of Environmental Sciences, University of East Anglia, Norwich Research Park, Norwich NR4 7TJ, UK

^c Ocean Biogeochemistry and Ecosystems, National Oceanography Centre Southampton, European Way, Southampton SO14 3ZH, UK

^d Alfred Wegener Institute, Helmholtz Centre for Polar and Marine Research, 27570 Bremerhaven, Germany

^e GEOMAR Helmholtz Centre for Ocean Research Kiel, Wischhofstraße 1-3, Build. 12, Kiel 24148, Germany

ARTICLE INFO

Keywords:

Carbon dioxide
Air-sea gas exchange
Marine carbonate system
Calcification

ABSTRACT

The ocean holds a large reservoir of carbon dioxide (CO₂), and mitigates climate change through uptake of anthropogenic CO₂. Fluxes of CO₂ between the atmosphere and surface ocean are regulated by a number of physical and biogeochemical processes, resulting in a spatiotemporally heterogeneous CO₂ distribution. Determining the influence of each individual process is useful for interpreting marine carbonate system observations, and is also necessary to investigate how changes in these drivers could affect air-sea CO₂ exchange. Biogeochemical processes exert an influence primarily through modifying seawater dissolved inorganic carbon (C_T) and total alkalinity (A_T), thus changing the seawater partial pressure of CO₂ (p_{sw}). Here, we propose a novel conceptual framework through which the size of the CO₂ source or sink generated by any biogeochemical process, denoted Φ, can be evaluated. This is based on the ‘isocapnic quotient’ (Q), which defines the trajectory through (A_T, C_T) phase space for which there is no change in p_{sw}. We discuss the limitations and uncertainties inherent in this technique, which are negligible for most practical purposes, and its links with existing, related approaches. We investigate the effect on Φ of spatiotemporal heterogeneity in Q in the present day surface ocean for several key biogeochemical processes. This leads the magnitude of the CO₂ source or sink generated by processes that modify A_T to vary spatiotemporally. Finally, we consider how the strength of each process as a CO₂ source or sink may change in a warmer, higher-CO₂ future ocean.

1. Introduction

The global ocean hosts a substantial reservoir of carbon dioxide (CO₂) in the form of dissolved inorganic carbon (C_T), which can buffer changes in the atmospheric CO₂ concentration (Le Quéré et al., 2016) and its climatic consequences (IPCC, 2013). Although the global surface ocean is presently a net CO₂ sink, the spatiotemporal distribution of air-sea CO₂ exchange is heterogeneous. To first order, CO₂ is supplied to the atmosphere in the tropics and upwelling zones, and taken up by the ocean in subpolar regions (Takahashi et al., 2009). The magnitude and phase of seasonal cycles in air-sea CO₂ exchange are also spatially variable. These patterns emerge from the interactions between a number of physical and biogeochemical processes. There are thus several reasons why we need to understand how each individual process affects air-sea CO₂ exchange, including interpreting *in situ* observations

of seawater chemistry, and projecting how changes in these drivers could affect the future oceanic CO₂ sink.

Marine processes can affect air-sea CO₂ exchange by altering the seawater partial pressure of CO₂ (p_{sw}), with increasing/decreasing p_{sw} tending to create a CO₂ source/sink, respectively, for atmospheric CO₂. One way that this can happen is through changes in seawater temperature and/or salinity (Weiss et al., 1982). Additionally, biogeochemical processes can modify p_{sw}, primarily through their effects on C_T and total alkalinity (A_T). The impact of changes in C_T is intuitive: if C_T is removed from solution (e.g. by conversion into organic matter), this creates the potential for additional CO₂ to be taken up from the atmosphere, thus reducing p_{sw}. A_T can qualitatively be thought of as the capacity of seawater to store C_T for a given value of p_{sw}. Processes that decrease A_T therefore increase p_{sw} and act as CO₂ sources to the atmosphere, while increasing A_T constitutes a CO₂ sink (Fig. 1).

* Corresponding author at: School of Environmental Sciences, University of East Anglia, Norwich Research Park, Norwich NR4 7TJ, UK.

E-mail addresses: matthew.humphreys@uea.ac.uk (M.P. Humphreys), Dieter.Wolf-Gladrow@awi.de (D.A. Wolf-Gladrow), Toby.Tyrrell@soton.ac.uk (T. Tyrrell), achterberg@geomar.de (E.P. Achterberg).

<https://doi.org/10.1016/j.marchem.2017.12.006>

Received 29 June 2017; Received in revised form 27 November 2017; Accepted 19 December 2017

0304-4203/ © 2017 The Authors. Published by Elsevier B.V. This is an open access article under the CC BY license (<http://creativecommons.org/licenses/by/4.0/>).

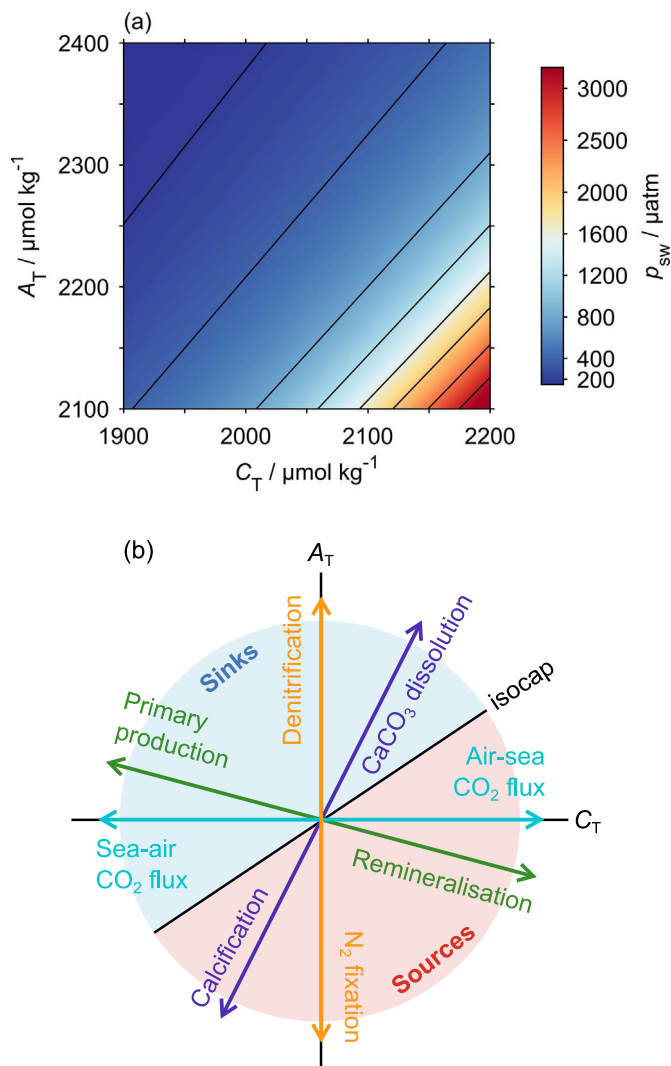


Fig. 1. (a) Distribution of p_{sw} in (A_T, C_T) phase space, calculated at temperature = 15°C and practical salinity = 35 using CO₂SYS (van Heuven et al., 2011). The black contours, called isocaps, are drawn at the p_{sw} values labelled on the colour bar. (b) Schematic trajectories of some example unit biogeochemical process vectors (\hat{q}). Vectors in the CO₂ ‘sources’ region (red shading) increase p_{sw} , while CO₂ ‘sinks’ (blue shading) decrease p_{sw} . The boundary between these regions is an isocap, and its slope is equal to the isocapnic quotient Q . (For interpretation of the references to colour in this figure legend, the reader is referred to the web version of this article.)

Consequently, there exists some ratio of changes in A_T and C_T that cancel out each other’s effect on p_{sw} , resulting in zero net p_{sw} change. We refer to this p_{sw} -neutral ratio as the ‘isocapnic quotient’ (Q). Its value varies through (A_T, C_T) phase space, and is equal to the slope of the p_{sw} isoline (or ‘isocap’) at any given point. We have appropriated the word ‘isocapnic’ from medical science, where it refers to a constant dissolved CO₂ concentration in blood, as there was no oceanographic term for this concept in seawater.

Here, we derive mathematical expressions for Q , and show how its value depends upon the state of the marine carbonate system. The changes in A_T and C_T driven by any biogeochemical process define its ‘biogeochemical process vector’ (\mathbf{q}). We introduce the parameter Φ , which combines Q and \mathbf{q} to quantify the potential size of the CO₂ source or sink associated with the biogeochemical process. Φ thereby indicates the amount of C_T that must be lost or gained by the seawater (e.g. through air-sea CO₂ exchange), following the action of a biogeochemical process, in order to return to the p_{sw} value from before the process occurred. The ‘released CO₂ to precipitated carbonate ratio’ (Ψ) defined by Frankignoulle et al. (1994) is a special case of Φ , applicable only to

calcification. We discuss the limitations and uncertainties associated with our approach, such as the assumption of isocap linearity, and timescale considerations. Our novel technique indicates that the CO₂ source or sink strength of any biogeochemical process that modifies A_T is not constant, but rather depends upon the local seawater conditions, in particular temperature and p_{sw} . We investigate the effect of spatio-temporal heterogeneity in Q in the surface ocean on Φ for different biogeochemical processes, using a climatological dataset that represents near-present day conditions (Takahashi et al., 2014b). Finally, we consider how these effects may change in a warmer, higher-CO₂ future ocean.

2. Methods

Throughout this article, square brackets indicate the dissolved concentration of the enclosed chemical species in mol kg^{-1} , where kg^{-1} is of seawater (not H₂O). In some instances, we use s and h to denote [CO_{2(aq)}] and [H⁺] respectively, for brevity. We exclusively use the Free pH scale throughout (i.e. $\text{pH} = -\log_{10} [\text{H}^+]$). The definitions of all symbols and abbreviations are summarised in Appendix A.

MATLAB functions that can be used to evaluate Q , Q_x and Φ (defined below), are freely available from <https://github.com/mvdh7/biogeochem-phi>.

2.1. The marine carbonate system

‘Dissolved inorganic carbon’ (C_T) is the sum of the aqueous CO₂, bicarbonate (HCO₃⁻) and carbonate (CO₃²⁻) ion concentrations (Zeebe and Wolf-Gladrow, 2001):

$$C_T = [\text{CO}_{2(\text{aq})}] + [\text{HCO}_3^-] + [\text{CO}_3^{2-}] \quad (1)$$

The reactions for the dynamic equilibria between the carbonate species in Eq. (1), and definitions of the relevant dissociation constants, are given in Appendix B.

Roughly speaking, ‘total alkalinity’ (A_T) quantifies the deficit of protons in solution relative to a ‘zero-level’ at pH around 4.5. More precisely, it is the excess of proton acceptors (like bicarbonate and carbonate ions) over proton donors with respect to a ‘zero level of protons’ (Dickson, 1981). The following simplified equation captures > 99.8% of its components in typical surface ocean seawater, which is sufficient for our purposes:

$$A_T = [\text{HCO}_3^-] + 2[\text{CO}_3^{2-}] + [\text{B}(\text{OH})_4^-] + [\text{OH}^-] - [\text{H}^+] \quad (2)$$

A_T is therefore influenced by chemical species additional to those directly related to CO₂. The relevant equations and reactions are given in Appendix B.

All of the marine carbonate system variables (e.g. C_T , A_T , p_{sw} or s , h) can be calculated if the values of any pair are known (Zeebe and Wolf-Gladrow, 2001).

2.2. Isocapnic quotient

The isocapnic quotient (Q) is defined as the rate of change of A_T relative to C_T at constant s (or equivalently p_{sw}), under constant salinity, temperature and pressure (STP) conditions:

$$Q = \left[\frac{\partial A_T}{\partial C_T} \right]_{s, \text{STP}} \quad (3)$$

2.2.1. Simple approximation

Before deriving the ‘exact’ equation for Q , we developed an informative approximation. Starting from the following simplified expressions for C_T and A_T :

$$C_T \approx C_x = [\text{HCO}_3^-] + [\text{CO}_3^{2-}] \quad (4)$$

$$A_T \approx A_x = [\text{HCO}_3^-] + 2[\text{CO}_3^{2-}] \quad (5)$$

we derived the following approximations for Q (i.e. Q_x), which are identical to each other, but stated in terms of p_{sw} and s respectively:

$$Q_x = 1 + \frac{2K_2 C_x}{K_0 K_1 p_{\text{sw}}} \quad (6)$$

$$Q_x = 1 + \frac{2K_2 C_x}{K_1 s} \quad (7)$$

The full derivation of Eqs. (6) and (7) is provided in Appendix C.

2.2.2. Full derivation

We derived the exact equation for Q from the definitions of C_T and A_T in Eqs. (1) and (2), as shown in Appendix D:

$$Q = \frac{(K_1 h s + 4K_1 K_2 s + K_w h + h^3)(K_B + h)^2 + K_B B_T h^3}{K_1 s (h + 2K_2)(K_B + h)^2} \quad (8)$$

We can thus use Eq. (8) to calculate Q , given any pair of marine carbonate system variables (Zeebe and Wolf-Gladrow, 2001).

2.3. Biogeochemical process vectors

The change in A_T relative to C_T during any given biogeochemical process can be quantified as a vector $\mathbf{q} = (A_q, C_q)$ through (A_T, C_T) phase space (Fig. 2). We use the notation $\hat{\mathbf{q}}$ to refer to the unit vector case (i.e. where \mathbf{q} has been normalised such that $A_q^2 + C_q^2 = 1$). In applying our method, it would normally be appropriate to use \mathbf{q} ; the unit $\hat{\mathbf{q}}$ simply provides a convenient way to normalise the different processes for our analysis. Previous studies have investigated these changes in detail (e.g. Wolf-Gladrow et al., 2007), so here we only provide A_q and C_q values associated with the selection of common processes described below, as examples (Table 1).

Air-sea CO_2 exchange increases or decreases C_T by the amount of CO_2 transferred (i.e. C_q), with no change in A_T (hence $A_q = 0$).

Table 1

A_q and C_q coefficients for the selection of biogeochemical processes schematically illustrated in Fig. 1b, following Wolf-Gladrow et al. (2007). Calculated both as \mathbf{q} (in this case, normalised to C_q or $A_q = \pm 1$) and $\hat{\mathbf{q}}$ (normalised by definition such that $A_q^2 + C_q^2 = 1$).

Process	\mathbf{q}		$\hat{\mathbf{q}}$	
	A_q	C_q	A_q	C_q
Air-to-sea CO_2 transfer	0	+1	0	+1
Sea-to-air CO_2 transfer	0	-1	0	-1
Autotrophic production	+0.21	-1	+0.21	-0.98
Remineralisation	-0.21	+1	-0.21	+0.98
Calcification	-2	-1	-0.89	-0.45
CaCO_3 dissolution	+2	+1	+0.89	+0.45
Denitrification ^a	+1	0	+1	0
N_2 fixation ^b	-1	0	-1	0

^a Denitrification and/or anammox.

^b N_2 fixation, followed by remineralisation and nitrate generation.

Autotrophic production converts C_T into particulate organic carbon (POC), so C_q for this process is stoichiometrically equal to the amount of POC formed. The associated increase in seawater A_T (i.e. A_q), of +0.21 mol per mol-C converted into POC, results from simultaneous nutrient uptake (Wolf-Gladrow et al., 2007). Calcification converts C_T into CaCO_3 , which decreases A_T by 2 mol per mol CaCO_3 formed (Eq. (2)). Remineralisation and CaCO_3 dissolution have opposite effects to autotrophic production and calcification respectively. Denitrification/anammox and N_2 fixation do not affect C_T (hence $C_q = 0$), but they alter A_T through nitrate uptake or production, in the same way as autotrophic production/remineralisation. N_2 fixation itself only converts N_2 into organic matter; this must be followed by remineralisation if A_T is to be decreased by nitrate production (Wolf-Gladrow et al., 2007). Therefore ‘ N_2 fixation’, here and throughout this article, refers to the complete process of N_2 fixation, followed by remineralisation and hence nitrate production.

2.4. CO_2 source/sink magnitude

We can use Q and any process vector \mathbf{q} to determine the excess of C_T generated by any biogeochemical process. In this context, the ‘excess of C_T ’ (denoted Φ) is defined as the amount of C_T that would need to be lost from the seawater following the action of a biogeochemical process, through an A_T -neutral process like air-sea gas exchange, in order for p_{sw} to return to its initial value (Fig. 2). This can be considered to represent the magnitude of the CO_2 source ($\Phi > 0$) or sink ($\Phi < 0$) generated by the process.

The geometry of Fig. 2 shows that Q satisfies:

$$Q = A_q / (C_q - \Phi) \quad (9)$$

which can trivially be rearranged to define Φ :

$$\Phi = C_q - A_q / Q \quad (10)$$

The units of Φ are the same as the units used for the inputs A_q and C_q to Eq. (10), which should be the same as each other (Appendix A). The notation $\hat{\Phi}$ is used where the CO_2 source/sink magnitude has been evaluated for the unit vector case (i.e. using $\hat{\mathbf{q}}$).

2.5. Investigating the isocapnic quotient distribution

We used the Takahashi et al. (2014b) surface ocean carbonate chemistry climatology to investigate the distribution of Q in the global surface ocean at the ‘present day’ (this climatology is normalised to the reference year 2005). Although this dataset is complete for sea surface temperature (SST), salinity and p_{sw} , it excludes A_T and C_T in the equatorial Pacific Ocean, because of high temporal variability driven by El Niño Southern Oscillation (Takahashi et al., 2014a). We filled this gap using CO_2SYS v1.1 (van Heuven et al., 2011) as follows. We used

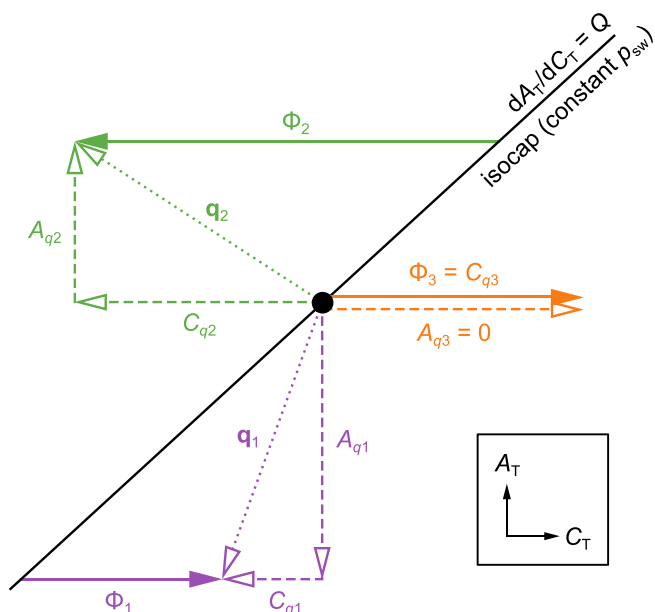


Fig. 2. Schematic of the geometric relationship between Q and Φ for three example biogeochemical processes. The dashed lines show the vector components A_q and C_q , dotted lines show the overall trajectories of \mathbf{q} (not shown for process 3), and solid lines show the corresponding Φ . Process 1 (purple, analogous to calcification) has negative A_{q1} and C_{q1} . This leads to an increase in C_T relative to the isocap value, and therefore positive Φ_1 – a CO_2 source. Process 2 (green, similar to primary production) also has negative C_{q2} but positive A_{q2} , leading to negative Φ_2 and a CO_2 sink. Process 3 (orange, like air-to-sea CO_2 transfer) has zero A_{q3} , and therefore $C_{q3} = \Phi_3$. (For interpretation of the references to colour in this figure legend, the reader is referred to the web version of this article.)

the climatological SST and salinity fields to predict A_T following Lee et al. (2006). C_T was calculated from these predicted A_T values, and p_{sw} , SST and salinity from the climatology. Silicate and phosphate concentrations, and pressure, were all set to zero.

We thence evaluated s from p_{sw} , SST and salinity using Henry's law (B.11). Next, h was calculated from s and C_T using Eq. (D.1). Finally, we determined both Q_x and Q from h and C_T using Eqs. (6) and (8) respectively, using the approximation $C_x = C_T$ in the former case Eq. (4). The coefficients necessary for these calculations were quantified following Weiss (1974) for K_0 , Lueker et al. (2000) for K_1 and K_2 , Dickson (1990b) for K_b , Lee et al. (2010) for B_T , and Dickson et al. (2007) for K_w . All dissociation constants reported on the Total pH scale were converted to the Free pH scale (Zeebe and Wolf-Gladrow, 2001) using the sulfate-to-chlorinity ratio of Morris and Riley (1966) and the bisulfate dissociation constant of Dickson (1990a).

We determined the relative importance of SST seasonality on Q at each grid point in the Takahashi et al. (2014b) dataset by evaluating Q using the monthly values for the SST, but with all other values held at their annual mean values. A similar procedure was followed to compute the seasonal influence of the marine carbonate system (i.e. p_{sw} and C_T) component, with SST instead held at its annual mean value, while p_{sw} and C_T were allowed to vary.

A caveat of our analysis based on this climatological dataset is that the spatiotemporal variability in Q in any specific individual year could exceed or fall short of that described here, because the dataset represents climatological mean conditions, normalised to the year 2005 (Takahashi et al., 2014a).

3. Results and discussion

3.1. The isocapnic quotient

3.1.1. Initial analysis of the approximation

We begin by briefly considering the Q_x approximation (Eq. (6)), which helps to later interpret the global distribution of Q . In the surface open ocean, C_T varies by a maximum of about 10% of its global mean concentration, whereas p_{sw} can vary by over 100% of its mean value (Takahashi et al., 2014a). Therefore Eq. (6) leads us to expect p_{sw} to be the dominant marine carbonate system control on Q , and we expect the spatiotemporal distributions of p_{sw} and Q to be inversely proportional to each other. However, Q_x is also dependent on the coefficients K_0 , K_1 and K_2 . Through their influence, we also expect temperature and salinity to modulate the Q distribution (Dickson et al., 2007). The factor K_2/K_0K_1 in Eq. (6) is positively correlated with both seawater temperature and salinity. Temperature has a stronger effect than salinity: across the range of temperatures commonly encountered in the global surface ocean, K_2/K_0K_1 increases by a factor of 6–7, while it grows by a factor of less than 2 across the equivalent salinity range. This suggests that SST will influence the Q distribution 6–7 times as strongly as either salinity or p_{sw} do.

We note that Q could also vary with depth through the influence of pressure on the equilibrium constants (Culberson et al., 1967). We do not investigate this pressure effect in detail here, because our focus is on air-sea CO_2 exchange in the near-surface ocean. In any case, this effect is small: moving from the sea surface to the deepest point in the ocean (Mariana Trench, pressure $\approx 1.1 \times 10^4$ dbar) reduces Q by $< 3\%$, if all other conditions (i.e. temperature, salinity, C_T and p_{sw}) are held constant. Accounting for this pressure influence, for both Q_x and Q , does not require any alterations to our equations. Rather, the effect of pressure should be included when evaluating the equilibrium/dissociation constants.

3.1.2. Annual mean state

Moving on to the 'exact' calculation (Eq. (8)), our analysis of 'present day' Q , calculated using the Takahashi et al. (2014b) climatological dataset, showed that the dominant controls on annual mean Q

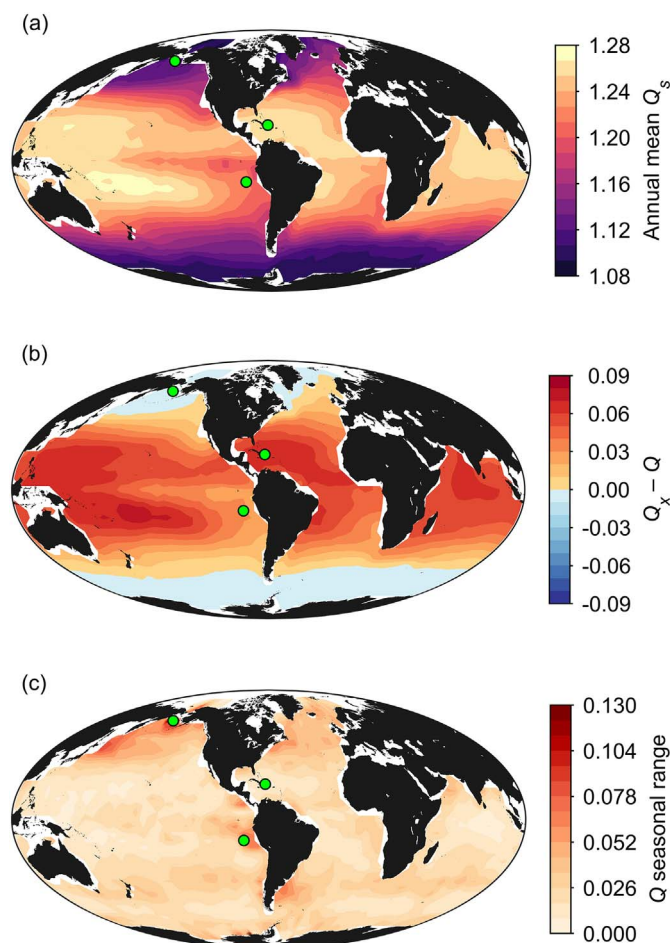


Fig. 3. (a) Annual mean Q , (b) difference between annual mean Q_x and Q , and (c) seasonal range of Q , all calculated from the climatological surface ocean dataset (Takahashi et al., 2014b). Note that in (c), the highest values (c. 0.13) exceed the colour scale range. The three green circles indicate the locations of the sites shown in Fig. 4. (For interpretation of the references to colour in this figure legend, the reader is referred to the web version of this article.)

throughout the global surface ocean are indeed SST and p_{sw} . Q has the expected positive correlation with SST, and inverse relationship with p_{sw} . Annual mean Q varies from a minimum around 1.08 at high latitudes to a maximum of nearly 1.28 in the tropics (Fig. 3a). This first order spatial distribution is dominantly driven by SST, but certain regions are also visibly influenced by p_{sw} . For example, high p_{sw} resulting from local upwelling (Wang et al., 2006) is responsible for the relatively low Q values observed in the eastern equatorial Pacific Ocean.

The approximation Q_x has a similar pattern to annual mean Q (Fig. 3b). They have roughly equal values at high latitudes, but Q_x tends to overestimate Q at higher SST values towards the equator, by up to 0.09 (c. 7%).

3.1.3. Seasonal variability

Some locations exhibit strong seasonal variability in Q , as quantified by the Q 'annual range' (Fig. 3c). This was defined as the difference between the maximum and minimum monthly Q at each grid point in the climatological dataset. The maximum Q annual range is about 0.13, which is almost half of the spatial range in the annual mean.

One striking feature is that the Q annual range is close to zero across large regions, for example the oligotrophic subtropical gyres (Fig. 3c). In these regions, the seasonal cycle of p_{sw} is dominantly controlled by SST-driven changes in K_0 , so SST and p_{sw} are positively correlated (Takahashi et al., 2009). We know from Section 3.1.1 that SST is positively correlated with Q , while p_{sw} has an inverse relationship with

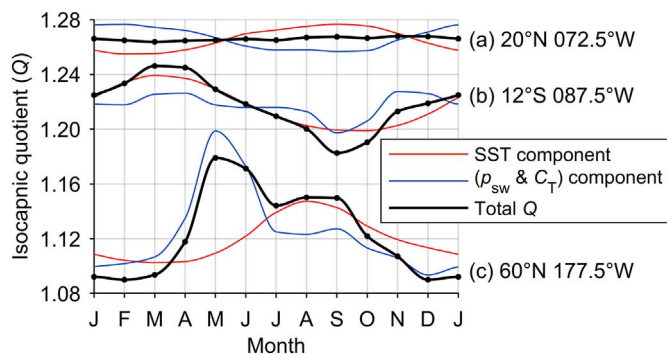


Fig. 4. Drivers of seasonal change in Q at selected sites from Fig. 3. (a) In the oligotrophic North Atlantic, the p_{sw} seasonal cycle is dominantly driven by SST, so their influences on Q compensate each other, leading to a small seasonal amplitude in Q . (b) Seasonal upwelling in the eastern equatorial Pacific drives high C_T and p_{sw} to accompany low SST, and these factors combine to drive relatively strong Q seasonality. (c) In the subpolar North Pacific, strong seasonal cycles in both SST and the marine carbonate system are slightly out of phase, leading to strong Q seasonality with dual maxima.

both. We would therefore expect this coupling of the SST and p_{sw} seasonal cycles to lead each to have opposing effects on Q , which could cancel each other out to some extent. Returning again the approximation Q_x , we found that the majority of the temperature sensitivity of the K_2/K_0K_1 factor in Eq. (6) is driven by K_0 . This therefore exactly cancels out the SST-driven K_0 effect on p_{sw} , as was further indicated by Eq. (7). The factor K_2/K_1 in Eq. (7) has much lower temperature sensitivity than K_2/K_0K_1 , and consequently the amplitude of Q seasonality is relatively low where SST is the dominant control on the seasonal p_{sw} cycle (Fig. 4a).

The isocapnic quotient therefore has a small seasonal range where p_{sw} seasonality is mainly controlled by SST, while large seasonal ranges are found where the p_{sw} and SST seasonal cycles are decoupled. Regions featuring seasonal upwelling of relatively cold, high- p_{sw} subsurface waters, such as the eastern equatorial Pacific (Wang et al., 2006), exhibit such decoupling (Fig. 4b). It is also observed in regions with high seasonal biological uptake of CO_2 , because primary production is more intense there during the warmer, lighter spring and summer months (Takahashi et al., 2009). Where the SST and p_{sw} cycles are not exactly in antiphase, this can also lead to multiple Q maxima within a single year (Fig. 4c).

3.2. CO_2 source/sink magnitude

The value of Φ quantifies the magnitude of the CO_2 source or sink. This is the amount of C_T that would need to be taken out of seawater (for positive Φ) in order to return to its original p_{sw} value, following the changes in A_T and C_T specified by \mathbf{q} . As changes to p_{sw} create the chemical gradients necessary to drive air-sea CO_2 fluxes, we have stated that Φ can be considered to represent the size of the CO_2 source or sink driven by \mathbf{q} . However, this interpretation assumes that the seawater is then given time to re-equilibrate back to its original p_{sw} value through air-sea CO_2 exchange, which may not always be the case. In Southern Ocean waters, for example, rapid subduction of water masses from the surface layer could terminate air-sea CO_2 exchange before the full CO_2 source or sink indicated by Φ has been realised (Ito and Follows, 2013). We might therefore more accurately describe Φ as the potential CO_2 source or sink. However, such fast subduction is not typical for the majority of the ocean, and CO_2 equilibration timescales for the ocean surface layer are typically on the order of a few months to a year (Jones et al., 2014), fast enough for re-equilibration to occur. Also, on much longer timescales, when these subducted waters eventually are returned to the ocean surface, the biogeochemically driven change in their CO_2 source or sink capacity should still be present. The rest of our discussion is therefore framed by the assumption that Φ does accurately represent

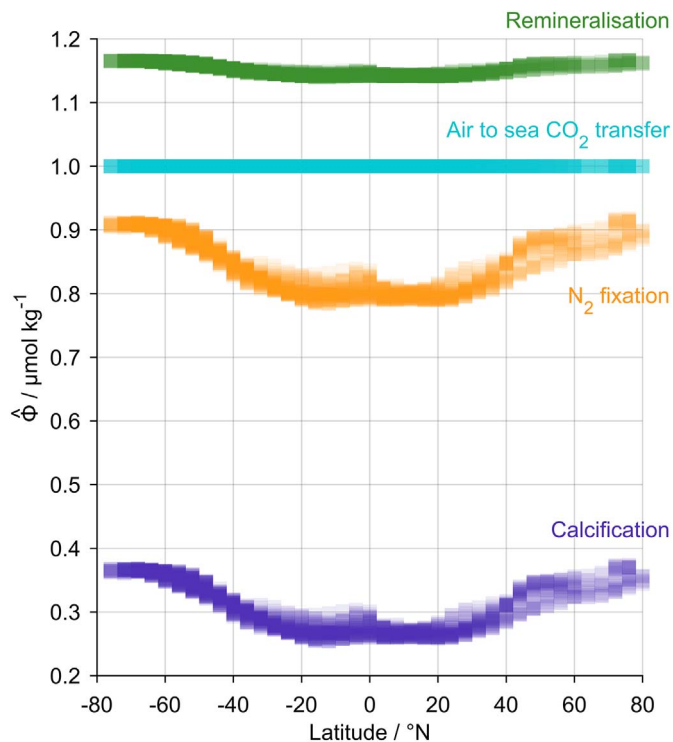


Fig. 5. Latitudinal distribution of $\hat{\Phi}$ in the Takahashi et al. (2014b) dataset for the CO_2 sources shown in Fig. 1. The biogeochemical process vectors (i.e. $\hat{\mathbf{q}}$) are from Table 1. Remineralisation is the strongest CO_2 source because its $\hat{\mathbf{q}}$ vector is closest to being perpendicular to Q , while calcification is the weakest as it is nearest to being parallel to Q . N_2 fixation has the greatest range, as it has the greatest A_q/C_q (i.e. $-\infty$), while air to sea CO_2 transfer is always exactly 1, because $A_q = 0$ and therefore $\Phi = C_q$ (Fig. 2). The plot for the equivalent CO_2 sink processes has the same appearance, but with all $\hat{\Phi}$ values multiplied by -1 .

the eventual magnitude of the CO_2 source or sink.

3.2.1. Sensitivity to Q

We can determine the sensitivity of Φ to changes in Q by considering Eq. (10). First, we can see that $\Phi \rightarrow C_q$ as $A_q \rightarrow 0$. In other words, if C_T is added to seawater with no change in A_T , then the amount of C_T that must be removed to return to the original p_{sw} (i.e. Φ) is simply equal to the amount of C_T that was added. Second, differentiation of Eq. (10) gives $d\Phi/dQ = A_q/Q^2$. Φ is therefore sensitive to Q for biogeochemical processes that modify A_T , and this sensitivity increases with the absolute value of A_q . Biogeochemical processes with greater absolute A_q/C_q thus exhibit greater spatiotemporal variability in Φ as a fraction of its mean value (Fig. 5).

Two key properties of $\hat{\Phi}$ can thus be intuitively predicted from A_q/C_q . First, the magnitude of $\hat{\Phi}$ is dictated by the geometric relationship between $\hat{\mathbf{q}}$ and Q (Fig. 2). $\hat{\Phi}$ is zero when the biogeochemical process vector is parallel to the isocap field, and therefore the slope of \mathbf{q} is equal to Q . $\hat{\Phi}$ reaches a maximum when $\hat{\mathbf{q}}$ is perpendicular to the isocap, when $A_q/C_q = -1/Q$. Second, the magnitude of the spatiotemporal variability in $\hat{\Phi}$ (driven by variability in Q) increases with the absolute value of A_q/C_q , and $\hat{\Phi}$ is homogeneous for processes with $A_q = 0$.

These properties can be illustrated by considering the latitudinal distribution of $\hat{\Phi}$ calculated from the climatological dataset for the CO_2 source processes shown in Fig. 1b and Table 1 (Fig. 5). In other words, we describe how the spatial distribution of Q in the climatology affects $\hat{\Phi}$ for each biogeochemical process in turn. Air-sea CO_2 exchange does not affect A_T , so its $\hat{\Phi}$ is uniformly equal to C_q (i.e. 1 for the unit vector case $\hat{\mathbf{q}}$) throughout the global ocean. The change in A_T associated with remineralisation is small relative to its C_q , leading to a modest range of $\hat{\Phi}$ (i.e. 1.13–1.17). The A_q value in this case moves $\hat{\mathbf{q}}$ more perpendicular to Q , resulting in greater mean $\hat{\Phi}$ than for air-sea CO_2 exchange.

Calcification and N_2 fixation both have greater A_q coefficients, and consequently greater ranges of $\hat{\Phi}$ (0.24–0.38 and 0.77–0.92 respectively). However, the mean $\hat{\Phi}$ for calcification is significantly smaller than for N_2 fixation, because \hat{q} for the former process is closer to being parallel to Q .

3.2.2. Timescale considerations

A key component of our conceptual framework is the biogeochemical process vector q . Some example values are suggested in Table 1, but these may not always be appropriate to use, depending on the timescale and context.

For example, consider the effect of combined organic matter and $CaCO_3$ production in the sea surface layer. On timescales of up to the lifetime of the particulate matter that is produced (e.g. days to weeks), the appropriate q would simply be the combination of the calcification and autotrophic production vectors from Table 1. However, on longer timescales (e.g. weeks to months), some of the particulate material may undergo remineralisation within the surface layer, while other components may sink into the abyss. On these timescales, material that is remineralised within the surface layer should be excluded from the calculation of q , as from the perspective of the seawater chemistry it has not been used up. For the hypothetical case where both primary production and calcification were occurring, but all organic matter was remineralised within the surface layer while all $CaCO_3$ was exported to depth, the appropriate q to use would simply be that for calcification.

Consequently, the correct combination of A_q and C_q values depends on (in these examples) export efficiencies and timescales of interest. Equivalent considerations also need to be made for other processes; for example, for N_2 fixation, the accuracy of our simplifying assumption that all fixed N_2 is remineralised into nitrate should be taken into account. The correct choice of A_q and C_q thus varies depending upon the nature of the scientific question being investigated, and is therefore left to the reader's discretion.

3.2.3. Deviation from linearity

Our equation for Φ (Eq. (10)) is such that the magnitude of Φ depends on the absolute A_q and C_q values, not just their ratio. For example, Φ calculated for $(A_q, C_q) = (4, 2)$ would be double that calculated for $(2, 1)$, despite both cases having the same $A_q : C_q$. Whatever the values of A_q and C_q , our calculation assumes that isocaps are linear in (A_T, C_T) phase space. This assumption is also implicit in the related concept of Ψ (Frankignoulle et al., 1994). However, Eq. (10) technically returns the instantaneous value of Φ , for infinitesimal A_q and C_q , and isocaps are in fact slightly curved. When calculated from large values of A_q and C_q , Φ therefore deviates from the correct result, which we call the ‘deviation from linearity’ (DfL, Fig. 6). Because of the direction of isocap curvature, the DfL is always negative, so Φ slightly underestimates the true CO_2 source/sink magnitude (Fig. 6b).

However, the magnitude of the DfL is likely to be negligible for many practical applications in open-ocean seawater. The DfL magnitude increased with the absolute value of A_q (Fig. 6b), and was insensitive to C_q . These properties were anticipated from our earlier discussion of the sensitivity of Q to A_q (Section 3.2.1). The DfL typically remains less than $1 \mu\text{mol kg}^{-1}$ for A_q values exceeding $\pm 200 \mu\text{mol kg}^{-1}$ (Fig. 6b). Given that an analytical precision of $\pm 2 \mu\text{mol kg}^{-1}$ is considered to represent a high quality oceanographic A_T and/or C_T measurement (Dickson et al., 2007), and that uncertainties in the rates of biological processes typically far exceed this value, we consider the uncertainty in Φ to be negligible in this context. The DfL is slightly greater (but still unimportant) at lower p_{sw} values (Fig. 6b), because the isocap curvature is greater under these conditions. The DfL is also slightly greater at low A_T values (by a factor of ≤ 2), but still negligible for most practical applications.

3.2.4. Lower limit for Q

The approximation Q_x helps to understand the reduced deviation

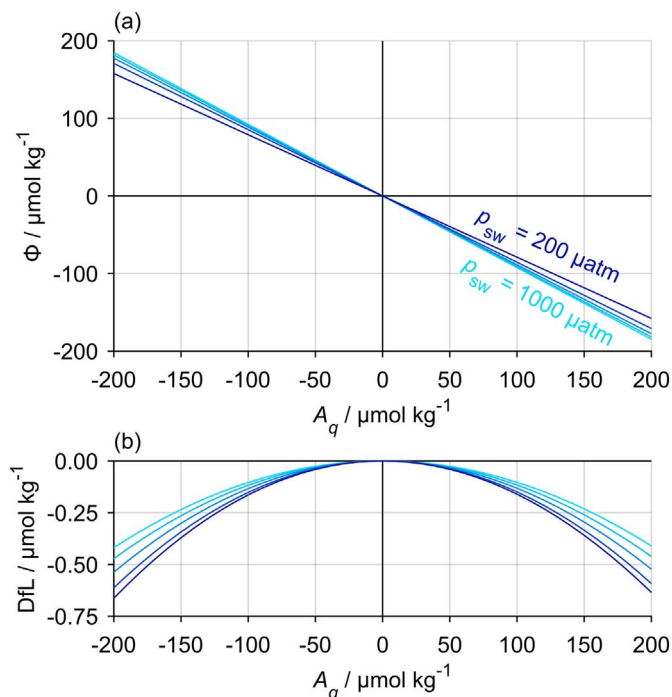


Fig. 6. Examples of the deviation from linearity (DfL) in Φ resulting from isocap curvature, at practical salinity = 35, temperature = 15°C , and $A_T = 2300 \mu\text{mol kg}^{-1}$. (a) Φ calculated from Eq. (10) across a range of A_q with $C_q = 0 \mu\text{mol kg}^{-1}$, at p_{sw} values increasing in intervals of $200 \mu\text{atm}$ from 200 (dark blue) to $1000 \mu\text{atm}$ (light blue). (b) Difference between Φ calculated from Eq. (10) and its exact value (i.e. the deviation from linearity, DfL), for the same data shown in (a). The deviation from linearity is zero when $A_q = 0$. At higher p_{sw} , isocaps are more linear, so the percentage error in Φ is smaller. Panel (b) would not be modified by changing C_q . (For interpretation of the references to colour in this figure legend, the reader is referred to the web version of this article.)

from linearity at high p_{sw} (Section 3.2.3), and also indicates a lower limit for Q as follows. All of the variables in Eqs. (6) and (7) are always positive. Furthermore, $[CO_{2(aq)}]$ cannot exceed C_T , by definition (1). Given these two facts, our approximation shows that the minimum possible value for Q occurs when the entirety of C_T is in aqueous CO_2 form, with no bicarbonate or carbonate ions present. Towards this point, $Q_x \rightarrow 1 + 2K_2/K_1$, which is virtually equal to 1 (more precisely, 1.0013 at 15°C and practical salinity = 35). This represents a ‘minimum buffering’ condition, occurring where $C_T \gg A_T$, and p_{sw} would be correspondingly very high. The Q lower limit of c. 1 makes sense intuitively as follows. Under these poorly buffered conditions, A_T would be dominated by the HCO_3^- term, and changes in s and C_T would be directly proportional to each other. An increase in A_T by 1 unit would thereby permit 1 unit of $CO_{2(aq)}$ to be converted into HCO_3^- . Returning to the original s , and therefore to the original p_{sw} , would therefore require 1 unit of CO_2 to be added to the seawater through air-sea gas exchange. For comparison, under more typical seawater conditions where $A_T \approx C_T$, the $[HCO_3^-]$ component represents only a fraction of any overall A_T change. A 1 unit increase in A_T would therefore involve conversion of less than 1 unit of $CO_{2(aq)}$, so less than 1 unit of CO_2 uptake will return p_{sw} to its original value, and therefore $Q > 1$. In typical open-ocean seawater, $[HCO_3^-]$ represents about 80% of A_T , so its Q is about 20% greater than 1.

3.3. Future impacts

Global mean surface ocean SST and p_{sw} are presently increasing (Wu et al., 2011; Tjiputra et al., 2014). Although these changes have opposing effects on Q , the p_{sw} trend dominates the Q response for an equilibrium climate sensitivity (i.e. the increase in global mean surface temperature induced by a doubling of p_{atm}) in the range from 1.5 to

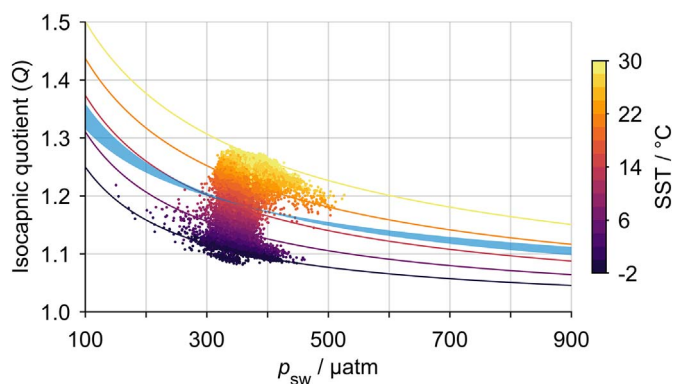


Fig. 7. Influence of p_{sw} and SST on Q . Scatter points show all surface ocean climatological data from Takahashi et al. (2014b). The curves at different SST values were calculated with constant global mean values of $A_T = 2300 \mu\text{mol kg}^{-1}$ and practical salinity = 35, and clearly show the inverse relationship between p_{sw} and Q predicted by Eq. (6). The blue shaded area indicates past and future trajectories of the global mean state corresponding to an equilibrium climate sensitivity of 1.5 to 4.5°C (IPCC, 2013), assuming constant A_T and salinity. (For interpretation of the references to colour in this figure legend, the reader is referred to the web version of this article.)

4.5°C (IPCC, 2013). Global mean Q is therefore likely to decrease as the ocean progresses towards a warmer, higher- CO_2 state (Fig. 7), at least until anthropogenic CO_2 emissions cease. After this point, Q may increase further as SST initially continues to rise, and then falls more slowly than p_{atm} (Solomon et al., 2009). Biogeochemical processes that decrease seawater A_T may thus become stronger sources of CO_2 . This positive feedback on p_{sw} has previously been identified specifically for calcification (Frankignoulle et al., 1994). Because of the opposing effects of SST and p_{sw} on Q , the smaller the climate sensitivity, the greater this positive feedback could be (Humphreys, 2017). Nevertheless, the size of this feedback moving into the future is likely to be modest, with global mean Q expected to decline from a mean value of about 1.18 at the Takahashi et al. (2014b) global mean p_{sw} of c. 360 μatm to 1.10 for a p_{sw} of 850 μatm (taking into account the associated warming), which is representative of the year 2100 under the ‘medium stabilisation’ anthropogenic CO_2 emissions scenario RCP6 (van Vuuren et al., 2011). For processes that only modify A_T (i.e. those that are most sensitive to Q , e.g. N_2 fixation and denitrification/anammox), this represents a 7.3% increase in the absolute value of $\hat{\Phi}$, while processes with smaller absolute A_q/C_q would be relatively less affected: 4.6% for calcification/ CaCO_3 dissolution, and 1.6% for primary production/remineralisation (see also Section 3.2.1).

However, this change applies to the magnitude of Φ , and in both directions: CO_2 sources with positive Φ will become stronger, but CO_2 sinks will also become stronger, with more negative Φ values. On timescales up to a few hundred years (i.e. shorter than whole-ocean mixing), the overall effect on air-sea CO_2 exchange may therefore depend on the depth distribution of each process relative to its counterpart. Marine primary production is focused within the surface mixed layer of the ocean, while a non-zero fraction of organic matter remineralisation typically occurs beneath this layer (Henson et al., 2012), from where it cannot directly influence air-sea gas exchange. The response to changing Q may therefore be a stronger CO_2 sink, driven by surface net community production, providing a negative feedback on p_{atm} . Similarly, net calcification mostly occurs within the euphotic surface layer (Poulton et al., 2006; Balch et al., 2011), while in the open ocean CaCO_3 dissolution is theoretically confined to relatively deep waters where CaCO_3 minerals are undersaturated (Morse et al., 2007). The CaCO_3 cycle may therefore act as a positive feedback on air-sea CO_2 exchange, dominated by the calcification (not dissolution) response to changes in Q . N_2 fixation is particularly concentrated in the thermocline

of the (sub)tropical oceans (Gruber and Sarmiento, 1997; Capone et al., 1997; Moisaner et al., 2010). However, A_T is not generated by this process until the organic matter thus formed has been remineralised into NO_3^- (Wolf-Gladrow et al., 2007), which may occur deeper still in the water column. The opposite processes of denitrification and anammox (Arrigo, 2005) are typically associated with poorly ventilated, subsurface oxygen minimum zones (Gruber and Sarmiento, 1997). It therefore seems unlikely that either process will strongly influence the ocean’s surface mixed layer, and it is unclear whether a positive or negative feedback would occur for this pair of processes.

4. Conclusions

We constructed a novel framework, built upon the ‘isocapnic quotient’ concept (i.e. Q), that allows us to systematically analyse the influence of any biogeochemical process that modifies the marine carbonate system over air-sea CO_2 exchange. The size of the CO_2 source or sink (to/from the atmosphere) generated by any such process (i.e. Φ) can be calculated from Q and the biogeochemical process vector $\mathbf{q} = (A_q, C_q)$. The vector \mathbf{q} quantifies the changes in seawater A_T and C_T driven by the biogeochemical process.

Analysis of ‘present day’ Q , calculated from a climatological dataset (Takahashi et al., 2014b), revealed spatial and seasonal variability in Q throughout the global surface ocean, mostly as a function of SST and p_{sw} . This means that the magnitude of the CO_2 source or sink generated by any specific biogeochemical process is similarly heterogeneous. Where the p_{sw} seasonal cycle is dominantly driven by SST, their effects on Q approximately cancel each other out, leading to a small seasonal range in Q . Stronger seasonal variability in Q can be observed where the p_{sw} and SST cycles are decoupled, for example by seasonal primary production or upwelling.

The sensitivity of Φ to Q increases with the absolute value of A_q/C_q , and Φ is simply equal to C_q when A_q is zero. Processes with greater A_q/C_q therefore have greater spatiotemporal variability in $\hat{\Phi}$. Processes with $\hat{\mathbf{q}}$ perpendicular to Q are the strongest CO_2 sources or sinks, while processes with $\hat{\mathbf{q}}$ parallel to Q are p_{sw} -neutral, and thus do not affect air-sea CO_2 exchange.

The buffer factor Ψ (Frankignoulle et al., 1994) is a special case of Φ , normalised to $C_q = -1$, and only applicable to calcification. Our Φ method, and its Ψ precursor, assume that isocaps are linear in (A_T, C_T) phase space, but they are actually slightly curved. However, the error in Φ resulting from this curvature is negligible for most practical applications, typically remaining under 0.5% for changes in A_T exceeding 100 $\mu\text{mol kg}^{-1}$.

We note that a similar approach to that taken here could be also applied to calculate the influence of biogeochemical processes over other marine carbonate system variables such as pH, $[\text{CO}_3^{2-}]$, and CaCO_3 mineral saturation states. However, it would be less obvious how to interpret the physical significance of the equivalent of Φ in these cases.

Based on an equilibrium climate sensitivity of up to 4.5°C, global mean Q is likely to decrease as anthropogenic CO_2 emissions continue. This will lead to biogeochemical processes that decrease seawater A_T becoming stronger sources of CO_2 to the atmosphere, while processes that increase A_T will become stronger CO_2 sinks.

Acknowledgements

We thank Andrew Yool, Alex Poulton, Jason Cole, and two anonymous reviewers for useful discussions on our method and this manuscript.

Funding: this work was supported by the Natural Environment Research Council, UK (grants NE/K00185X/1 and NE/K002546/1).

Appendix A. Summary of symbols

Table A.2

Summary of symbols and abbreviations used in this manuscript.

Symbol	Variable (and relevant equation)	Units
A_T	Total alkalinity (Eq. (2))	mol kg^{-1}
A_q	Change in A_T associated with a process	mol kg^{-1}
A_x	Approximation of A_T (Eq. (5))	mol kg^{-1}
B_T	Dissolved boric acid (Eq. (B.5))	mol kg^{-1}
C_T	Dissolved inorganic carbon (Eq. (1))	mol kg^{-1}
C_q	Change in C_T associated with a process	mol kg^{-1}
C_x	Approximation of C_T (Eq. (4))	mol kg^{-1}
DfL	Deviation from linearity (Section 3.2.3)	mol kg^{-1}
F	Sea-to-air CO_2 flux (Eq. (B.12))	mol m^{-2}
h	Hydrogen ion concentration, $[\text{H}^+]$	mol kg^{-1}
K_0	Stoichiometric equilibrium constant for CO_2 dissolution (Eq. (B.11))	$\text{mol kg}^{-1} \text{ atm}^{-1}$
K_1	First carbonic acid stoichiometric dissociation constant (Eq. (B.3))	mol kg^{-1}
K_2	Second carbonic acid stoichiometric dissociation constant (Eq. (B.4))	mol kg^{-1}
K_B	Boric acid stoichiometric dissociation constant (Eq. (B.7))	mol kg^{-1}
K_w	Stoichiometric ion product of water (Eq. (B.9))	$\text{mol}^2 \text{ kg}^{-2}$
p_{sw}	Seawater CO_2 partial pressure (Eq. (B.11))	atm
p_{atm}	Atmospheric CO_2 partial pressure (Eq. (B.11))	atm
\mathbf{q}	Biogeochemical process vector (A_q, C_q)	mol kg^{-1}
$\hat{\mathbf{q}}$	Unit \mathbf{q} (normalised such that $A_q^2 + C_q^2 = 1$)	mol kg^{-1}
s	Aqueous CO_2 concentration, $[\text{CO}_{2(\text{aq})}]$	mol kg^{-1}
Q	Isocapnic quotient (Eq. (D.5))	–
Q_x	Approximation of Q based on A_x and C_x (Eq. (C.8))	–
Tr	Gas transfer velocity (Eq. (B.12))	$\text{mol atm}^{-1} \text{ m}^{-2}$
β	Shorthand for $p_{\text{sw}}K_0K_1/K_2$ (Eqs. (C.5)–(C.8))	mol kg^{-1}
Φ	Size of CO_2 source/sink driven by a process (Eq. (10))	mol kg^{-1}
$\hat{\Phi}$	Φ for the unit vector case (i.e. $\hat{\mathbf{q}}$)	mol kg^{-1}
Ψ	Special case of Φ for calcification ^a	–

^a See Frankignoulle et al. (1994).

Appendix B. Marine carbonate system equilibria

The reactions for the dynamic equilibria between the carbonate species in Eq. (1) can be represented as:



where the stoichiometric dissociation coefficients K_1 and K_2 , which can be estimated using empirical functions of temperature, salinity and pressure (Dickson et al., 2007), are given by:

$$K_1 = [\text{H}^+][\text{HCO}_3^-]/[\text{CO}_{2(\text{aq})}] \quad (\text{B.3})$$

$$K_2 = [\text{H}^+][\text{CO}_3^{2-}]/[\text{HCO}_3^-] \quad (\text{B.4})$$

For boric acid, the relevant equations are:

$$B_T = [\text{B}(\text{OH})_3] + [\text{B}(\text{OH})_4^-] \quad (\text{B.5})$$



$$K_B = [\text{H}^+][\text{B}(\text{OH})_4^-]/[\text{B}(\text{OH})_3] \quad (\text{B.7})$$

and for the dissociation of water into protons and hydroxide ions:



$$K_w = [\text{H}^+][\text{OH}^-] \quad (\text{B.9})$$

Dissolution of CO_2 into seawater can be represented by the following reaction:



The direction of net air-sea CO_2 transfer is determined by the partial pressure of CO_2 in seawater (p_{sw}) relative to its atmospheric value (p_{atm}).

Seawater p_{sw} is directly proportional to $[\text{CO}_{2(aq)}]$, following Henry's law for CO_2 :

$$p_{sw} = [\text{CO}_{2(aq)}]/K_0 \quad (\text{B.11})$$

where the solubility coefficient K_0 is a function of seawater temperature and salinity (Weiss, 1974). The net sea-to-air CO_2 flux (F) is then given by:

$$F = \text{Tr} (p_{sw} - p_{atm}) \quad (\text{B.12})$$

where Tr is the gas transfer velocity (also known as the 'piston velocity'), which can be parameterised as a function of wind speed, temperature and salinity (e.g. Wanninkhof, 2014). Processes that increase p_{sw} are therefore considered to be sources for atmospheric CO_2 , for they will shift the value of $(p_{sw} - p_{atm})$ in favour of ocean to atmosphere CO_2 transfer. Conversely, processes that decrease p_{sw} are CO_2 sinks, enhancing seawater CO_2 uptake.

Appendix C. Isocapnic quotient approximation

We derived the approximation to the isocapnic quotient Q (i.e. Q_x) as follows. First, we combined Eqs. (B.3), (B.4) and (B.11) to produce the following expression for p_{sw} :

$$p_{sw} = \frac{K_2 [\text{HCO}_3^-]^2}{K_0 K_1 [\text{CO}_3^{2-}]} \quad (\text{C.1})$$

Then, using the approximations (4) and (5) for C_T and A_T respectively, we derived equations for $[\text{HCO}_3^-]$ and $[\text{CO}_3^{2-}]$ in terms of C_x and A_x :

$$[\text{HCO}_3^-] = 2C_x - A_x \quad (\text{C.2})$$

$$[\text{CO}_3^{2-}] = A_x - C_x \quad (\text{C.3})$$

The approximations (4) and (5) are reasonably accurate, as the $[\text{HCO}_3^-]$ and $[\text{CO}_3^{2-}]$ terms together typically represent over 99% of C_T and over 97% of A_T .

Next, we substituted Eqs. (C.2) and (C.3) into Eq. (C.1):

$$p_{sw} = \frac{K_2 (2C_x - A_x)^2}{K_0 K_1 (A_x - C_x)} \quad (\text{C.4})$$

This is a quadratic equation for A_x , which we rearranged as follows:

$$\begin{aligned} (2C_x - A_x)^2 &= \beta (A_x - C_x) \\ 4(C_x)^2 - 4C_x A_x + (A_x)^2 &= \beta A_x - \beta C_x \\ (A_x)^2 - (4C_x + \beta)A_x &= -[4(C_x)^2 + \beta C_x] \end{aligned} \quad (\text{C.5})$$

where β is shorthand for $p_{sw} K_0 K_1 / K_2$. We used the quadratic formula to solve Eq. (C.5):

$$A_x = 2C_x + \frac{\beta}{2} \pm \sqrt{\frac{\beta^2}{4} + \beta C_x} \quad (\text{C.6})$$

The solution of Eq. (C.6) with the negative square root term gives realistic values for A_x . We simplified this further using a Taylor series expansion:

$$\begin{aligned} A_x &= 2C_x + \frac{\beta}{2} - \sqrt{\frac{\beta^2}{4} + \beta C_x} \\ &= 2C_x + \frac{\beta}{2} - \frac{\beta}{2} \sqrt{1 + \frac{4C_x}{\beta}} \\ &\approx 2C_x + \frac{\beta}{2} - \frac{\beta}{2} \left[1 + \frac{2C_x}{\beta} - \frac{2(C_x)^2}{\beta^2} \right] \\ &= C_x \left(1 + \frac{C_x}{\beta} \right) \end{aligned} \quad (\text{C.7})$$

Finally, we differentiated Eq. (C.7) with respect to C_x to find an approximation for Q (i.e. Q_x):

$$Q_x = \frac{\partial A_x}{\partial C_x} = 1 + \frac{2C_x}{\beta} = 1 + \frac{2K_2 C_x}{K_0 K_1 p_{sw}} \quad (\text{C.8})$$

This can be converted into a function of s , rather than p_{sw} , by using Eq. (B.11):

$$Q_x = 1 + \frac{2K_2 C_x}{K_1 s} \quad (\text{C.9})$$

Eqs. (C.8) and (C.9) are identical to Eqs. (6) and (7) respectively in the main text.

Appendix D. Exact isocapnic quotient

To derive an exact equation for Q , we first converted Eqs. (1) and (2) into functions of h and s . Thus we rearranged Eqs. (B.3) and (B.4) and substituted into Eq. (1) to find C_T :

$$C_T = s \left(1 + \frac{K_1}{h} + \frac{K_1 K_2}{h^2} \right) \quad (\text{D.1})$$

Similarly, we rearranged Eqs. (B.3), (B.4), (B.7) and (B.9) and substituted into Eq. (2) to find A_T :

$$A_T = \frac{K_1 s}{h} + \frac{2K_1 K_2 s}{h^2} + \frac{K_B B_T}{K_B + h} + \frac{k_w}{h} - h \quad (\text{D.2})$$

We then differentiated each of Eqs. (D.1) and (D.2) with respect to h at constant s :

$$\begin{aligned} \frac{\partial C_T}{\partial h} &= -s \left(\frac{K_1}{h^2} + \frac{2K_1 K_2}{h^3} \right) \\ &= \frac{K_1 s (h + 2K_2)}{-h^3} \end{aligned} \quad (\text{D.3})$$

$$\begin{aligned} \frac{\partial A_T}{\partial h} &= - \left(\frac{K_1 s}{h^2} + \frac{4K_1 K_2 s}{h^3} + \frac{K_B B_T}{(K_B + h)^2} + \frac{K_w}{h^2} + 1 \right) \\ &= \frac{(K_1 h s + 4K_1 K_2 s + K_w h + h^3)(K_B + h)^2 + K_B B_T h^3}{-h^3 (K_B + h)^2} \end{aligned} \quad (\text{D.4})$$

Finally, we applied the chain rule to determine Q (i.e. $\partial A_T / \partial C_T$ at constant s) in terms of h and s :

$$Q = \frac{(K_1 h s + 4K_1 K_2 s + K_w h + h^3)(K_B + h)^2 + K_B B_T h^3}{K_1 s (h + 2K_2)(K_B + h)^2} \quad (\text{D.5})$$

We can then use Eq. (D.5), which is identical to Eq. (8) in the main text, to calculate Q given any pair of marine carbonate system variables (Zeebe and Wolf-Gladrow, 2001).

References

- Arrigo, K.R., 2005. Marine microorganisms and global nutrient cycles. *Nature* 437 (7057), 349–355. <http://dx.doi.org/10.1038/nature04159>.
- Balch, W.M., Drapeau, D.T., Bowler, B.C., Lyczowski, E., Booth, E.S., Alley, D., 2011. The contribution of coccolithophores to the optical and inorganic carbon budgets during the Southern Ocean Gas Exchange Experiment: new evidence in support of the “Great Calcite Belt” hypothesis. *J. Geophys. Res. Oceans* 116 (C4), C00F06. <http://dx.doi.org/10.1029/2011JC006941>.
- Capone, D.G., Zehr, J.P., Paerl, H.W., Bergman, B., Carpenter, E.J., 1997. Trichodesmium, a globally significant marine cyanobacterium. *Science* 276 (5316), 1221–1229. <http://dx.doi.org/10.1126/science.276.5316.1221>.
- Culbertson, C., Kester, D.R., Pytkowicz, R.M., 1967. High-pressure dissociation of carbonic and boric acids in seawater. *Science* 157 (3784), 59–61.
- Dickson, A.G., 1981. An exact definition of total alkalinity and a procedure for the estimation of alkalinity and total inorganic carbon from titration data. *Deep-Sea Res.* 28 (6), 609–623. [http://dx.doi.org/10.1016/0198-0149\(81\)90121-7](http://dx.doi.org/10.1016/0198-0149(81)90121-7).
- Dickson, A.G., 1990a. Standard potential of the reaction: $\text{AgCl}_{(s)} + 0.5\text{H}_{2(g)} = \text{Ag}_{(s)} + \text{HCl}_{(aq)}$, and the standard acidity constant of the ion HSO_4^- in synthetic sea water from 273.15 to 318.15 K. *J. Chem. Thermodyn.* 22 (2), 113–127. [http://dx.doi.org/10.1016/0021-9614\(90\)90074-Z](http://dx.doi.org/10.1016/0021-9614(90)90074-Z).
- Dickson, A.G., 1990b. Thermodynamics of the dissociation of boric acid in synthetic seawater from 273.15 to 318.15 K. *Deep-Sea Res.* 37 (5), 755–766. [http://dx.doi.org/10.1016/0198-0149\(90\)90004-F](http://dx.doi.org/10.1016/0198-0149(90)90004-F).
- Dickson, A.G., Sabine, C.L., Christian, J.R. (Eds.), 2007. *Guide to Best Practices for Ocean CO₂ Measurements*. PICES Special Publication 3.
- Frankignoulle, M., Canon, C., Gattuso, J.-P., 1994. Marine calcification as a source of carbon dioxide: positive feedback of increasing atmospheric CO₂. *Limnol. Oceanogr.* 39 (2), 458–462. <http://dx.doi.org/10.4319/lo.1994.39.2.0458>.
- Gruber, N., Sarmiento, J.L., 1997. Global patterns of marine nitrogen fixation and denitrification. *Global Biogeochem. Cy.* 11 (2), 235–266. <http://dx.doi.org/10.1029/97GB00077>.
- Henson, S.A., Sanders, R., Madsen, E., 2012. Global patterns in efficiency of particulate organic carbon export and transfer to the deep ocean. *Glob. Biogeochem. Cycles* 26, GB1028. <http://dx.doi.org/10.1029/2011GB004099>.
- Humphreys, M.P., 2017. Climate sensitivity and the rate of ocean acidification: future impacts, and implications for experimental design. *ICES J. Mar. Sci.* 74 (4), 934–940. <http://dx.doi.org/10.1093/icesjms/fsw189>.
- IPCC, 2013. *Climate Change 2013: The Physical Science Basis. Contribution of Working Group I to the Fifth Assessment Report of the Intergovernmental Panel on Climate Change*. Cambridge University Press, Cambridge, UK. <http://dx.doi.org/10.1017/CBO9781107415324>.
- Ito, T., Follows, M.J., 2013. Air-sea disequilibrium of carbon dioxide enhances the biological carbon sequestration in the Southern Ocean. *Global Biogeochem. Cy.* 27, 1–10. <http://dx.doi.org/10.1002/2013GB004682>.
- Jones, D.C., Ito, T., Takano, Y., Hsu, W.-C., 2014. Spatial and seasonal variability of the air-sea equilibration timescale of carbon dioxide. *Glob. Biogeochem. Cycles* 28 (11), 1163–1178. <http://dx.doi.org/10.1002/2014GB004813>.
- Le Quéré, C., Andrew, R.M., Canadell, J.G., Sitch, S., Korsbakken, J.I., Peters, G.P., Manning, A.C., Boden, T.A., Tans, P.P., Houghton, R.A., Keeling, R.F., Alin, S., Andrews, O.D., Anthoni, P., Barbero, L., Bopp, L., Chevallier, F., Chini, L.P., Ciais, P., Currie, K., Delire, C., Doney, S.C., Friedlingstein, P., Gkritzalis, T., Harris, I., Hauck, J., Haverd, V., Hoppema, M., Klein Goldewijk, K., Jain, A.K., Kato, E., Körtzinger, A., Landschützer, P., Lefèvre, N., Lenton, A., Lienert, S., Lombardozi, D., Melton, J.R., Metz, N., Millero, F., Monteiro, P.M.S., Munro, D.R., Nabel, J.E.M.S., Nakaoka, S.-I., O'Brien, K., Olsen, A., Omar, A.M., Ono, T., Pierrot, D., Poulter, B., Rödenbeck, C., Salisbury, J., Schuster, U., Schwinger, J., Séférian, R., Skjelvan, I., Stocker, B.D., Sutton, A.J., Takahashi, T., Tian, H., Tilbrook, B., van der Laan-Luijkx, I.T., van der Werf, G.R., Viovy, N., Walker, A.P., Wiltshire, A.J., Zaehle, S., 2016. Global Carbon Budget 2016. *Earth Syst. Sci. Data* 8 (2), 605–649. <http://dx.doi.org/10.5194/essd-8-605-2016>.
- Lee, K., Kim, T.-W., Byrne, R.H., Millero, F.J., Feely, R.A., Liu, Y.-M., 2010. The universal ratio of boron to chlorinity for the North Pacific and North Atlantic oceans. *Geochim. Cosmochim. Acta* 74 (6), 1801–1811. <http://dx.doi.org/10.1016/j.gca.2009.12.027>.
- Lee, K., Tong, L.T., Millero, F.J., Sabine, C.L., Dickson, A.G., Goyet, C., Park, G.-H., Wanninkhof, R., Feely, R.A., Key, R.M., 2006. Global relationships of total alkalinity with salinity and temperature in surface waters of the world's oceans. *Geophys. Res. Lett.* 33 (19), L19605. <http://dx.doi.org/10.1029/2006GL027207>.
- Lueker, T.J., Dickson, A.G., Keeling, C.D., 2000. Ocean pCO₂ calculated from dissolved inorganic carbon, alkalinity, and equations for k_1 and k_2 : validation based on laboratory measurements of CO₂ in gas and seawater at equilibrium. *Mar. Chem.* 70 (1–3), 105–119. [http://dx.doi.org/10.1016/S0304-4203\(00\)00022-0](http://dx.doi.org/10.1016/S0304-4203(00)00022-0).
- Moisander, P.H., Beinart, R.A., Hewson, I., White, A.E., Johnson, K.S., Carlson, C.A., Montoya, J.P., Zehr, J.P., 2010. Unicellular cyanobacterial distributions broaden the oceanic N₂ fixation domain. *Science* 327 (5972), 1512–1514. <http://dx.doi.org/10.1126/science.1185468>.
- Morris, A.W., Riley, J.P., 1966. The bromide/chlorinity and sulphate/chlorinity ratio in sea water. *Deep-Sea Res.* 13 (4), 699–705. [http://dx.doi.org/10.1016/0011-7471\(66\)90601-2](http://dx.doi.org/10.1016/0011-7471(66)90601-2).
- Morse, J.W., Arvidson, R.S., Lüttge, A., 2007. Calcium carbonate formation and dissolution. *Chem. Rev.* 107 (2), 342–381. <http://dx.doi.org/10.1021/cr050358j>.
- Poulton, A.J., Sanders, R., Holligan, P.M., Stinchcombe, M.C., Adey, T.R., Brown, L., Chamberlain, K., 2006. Phytoplankton mineralization in the tropical and subtropical Atlantic Ocean. *Global Biogeochem. Cy.* 20 (4), GB4002. <http://dx.doi.org/10.1029/2006GB002712>.
- Solomon, S., Plattner, G.-K., Knutti, R., Friedlingstein, P., 2009. Irreversible climate change due to carbon dioxide emissions. *Proc. Natl. Acad. Sci. U.S.A.* 106 (6), 1704–1709. <http://dx.doi.org/10.1073/pnas.0812721106>.
- Takahashi, T., Sutherland, S.C., Chipman, D.W., Goddard, J.G., Ho, C., Newberger, T., Sweeney, C., Munro, D.R., 2014a. Climatological distributions of pH, pCO₂, total CO₂, alkalinity, and CaCO₃ saturation in the global surface ocean, and temporal changes at selected locations. *Mar. Chem.* 164, 95–125. <http://dx.doi.org/10.1016/j.marchem.2014.06.004>.
- Takahashi, T., Sutherland, S.C., Chipman, D.W., Goddard, J.G., Newberger, T., Sweeney, C., 2014b. Climatological Distributions of pH, pCO₂, Total CO₂, Alkalinity, and CaCO₃ Saturation in the Global Surface Ocean. ORNL/CDIAC-160, NDP-094, Carbon Dioxide Information Analysis Center. Oak Ridge National Laboratory, U.S. Department of Energy, Oak Ridge, Tennessee <http://dx.doi.org/10.3334/CDIAC/OTG.NDP094>.
- Takahashi, T., Sutherland, S.C., Wanninkhof, R., Sweeney, C., Feely, R.A., Chipman, D.W., Hales, B., Friederich, G., Chavez, F., Sabine, C., Watson, A., Bakker, D.C.E., Schuster, U., Metz, N., Yoshikawa-Inoue, H., Ishii, M., Midorikawa, T., Nojiri, Y., Körtzinger, A., Steinhoff, T., Hoppema, M., Olafsson, J., Arnarson, T.S., Tilbrook, B., Johannessen, T., Olsen, A., Bellerby, R., Wong, C.S., Delille, B., Bates, N.R., de Baar, H., 2009. Climatological mean and decadal change in surface ocean pCO₂, and net sea-air CO₂ flux over the global oceans. *Deep-Sea Res. Pt II* 56, 554–577. <http://dx.doi.org/10.1016/j.dsr2.2008.12.009>.
- Tjiputra, J.F., Olsen, A., Bopp, L., Lenton, A., Pfeil, B., Roy, T., Segsneider, J., Totterdell, I., Heinze, C., 2014. Long-term surface pCO₂ trends from observations and

- models. *Tellus B* 66, 23083. <http://dx.doi.org/10.3402/tellusb.v66.23083>.
- van Heuven, S., Pierrot, D., Rae, J.W.B., Lewis, E., Wallace, D.W.R., 2011. CO₂SYS v 1.1, MATLAB Program Developed for CO₂ System Calculations. ORNL/CDIAC-105b. Carbon Dioxide Information Analysis Center, Oak Ridge National Laboratory, U.S. Department of Energy, Oak Ridge, Tennessee.
- van Vuuren, D.P., Edmonds, J., Kainuma, M., Riahi, K., Thomson, A., Hibbard, K., Hurtt, G.C., Kram, T., Krey, V., Lamarque, J.-F., Masui, T., Meinshausen, M., Nakicenovic, N., Smith, S.J., Rose, S.K., 2011. The representative concentration pathways: an overview. *Clim. Chang.* 109 (1-2), 5–31. <http://dx.doi.org/10.1007/s10584-011-0148-z>.
- Wang, X., Christian, J.R., Murtugudde, R., Busalacchi, A.J., 2006. Spatial and temporal variability of the surface water pCO₂ and air-sea CO₂ flux in the equatorial Pacific during 1980–2003: a basin-scale carbon cycle model. *J. Geophys. Res.* 111, C07S04. <http://dx.doi.org/10.1029/2005JC002972>.
- Wanninkhof, R., 2014. Relationship between wind speed and gas exchange over the ocean revisited: gas exchange and wind speed over the ocean. *Limnol. Oceanogr. Methods* 12 (6), 351–362. <http://dx.doi.org/10.4319/lom.2014.12.351>.
- Weiss, R.F., 1974. Carbon dioxide in water and seawater: the solubility of a non-ideal gas. *Mar. Chem.* 2 (3), 203–215. [http://dx.doi.org/10.1016/0304-4203\(74\)90015-2](http://dx.doi.org/10.1016/0304-4203(74)90015-2).
- Weiss, R.F., Jahnke, R.A., Keeling, C.D., 1982. Seasonal effects of temperature and salinity on the partial pressure of CO₂ in seawater. *Nature* 300 (5892), 511–513. <http://dx.doi.org/10.1038/300511a0>.
- Wolf-Gladrow, D.A., Zeebe, R.E., Klaas, C., Körtzinger, A., Dickson, A.G., 2007. Total alkalinity: the explicit conservative expression and its application to biogeochemical processes. *Mar. Chem.* 106 (1-2), 287–300. <http://dx.doi.org/10.1016/j.marchem.2007.01.006>.
- Wu, Z., Huang, N.E., Wallace, J.M., Smoliak, B.V., Chen, X., 2011. On the time-varying trend in global-mean surface temperature. *Clim. Dyn.* 37 (3-4), 759–773. <http://dx.doi.org/10.1007/s00382-011-1128-8>.
- Zeebe, R.E., Wolf-Gladrow, D., 2001. CO₂ in Seawater: Equilibrium, Kinetics, Isotopes. Elsevier Oceanography Series, vol. 65 Elsevier Ltd, Oxford, UK.